 doi:10.20944/preprints202210.0162.v1

Article

Electrochemical Immunosensor Based on Carboxylated Graphene/SPCE for Igg-SARS-Cov-2 Nucleocapsid Determination

Luciana Freire[1], Camila Ruzo[1], Barbara Salgado[2], Ariamna María Dip Gandarilla[1], Yonny Romaguera-Barcelay [1,3], Ana P.M. Tavares[3], MGF Sales[3], Isabelle Cordeiro[1], Jaila Lalwani[1], Robert Matos[4], Henrique Fonseca Filho[5], Spartaco Astofi-Filho[1], Ştefan Ţălu[6], Pritesh Lalwani[1,2], Walter Ricardo Brito[1] *

[1] Department of Chemistry, Institute of Exact Sciences, Federal University of Amazonas, Manaus, Amazonas 69067-005, Brazil.
[2] Instituto Leônidas e Maria Deane (ILMD), Fiocruz Amazônia, Manaus, Amazonas, Brazil
[3] BioMark@UC, Department of Chemical Engineering, Faculty of Sciences and Technology, University of Coimbra, Coimbra, 3030-790, Portugal.
[4] Amazonian Materials Group, Federal University of Amapá (UNIFAP), Macapá/AP, Brazil.
[5] Laboratory of Nanomaterials Synthesis and Nanoscopy (LSNN), Federal University of Amazonas (UFAM), Manaus 69067-005, AM, Brazil.
[6] The Technical University of Cluj-Napoca, The Directorate of Research, Development and Innovation Management (DMCDI), Constantin Daicoviciu Street, no. 15, Cluj-Napoca, 400020, Cluj county, Romania,
* Corresponding author: wrbrito@ufam.edu.br; +55 92981379920

Abstract: The COVID-19 pandemic has highlighted the importance and urgent need of rapid and accurate diagnostic tests for detection and screening of this infection. In our proposal, a biosensor based on the ELISA immunoassay was developed for monitoring antibodies against SARS-CoV-2 in human serum samples. The SARS-CoV-2 nucleocapsid protein (N-protein) was selected as a specific receptor for the detection of SARS-CoV-2 nucleocapsid immunoglobulin G. Thus, the N-protein was immobilized on surface of screen-printed carbon electrode (SPCE) modified with carboxylated graphene (CG). The IgG-SARS-CoV-2 nucleocapsid concentration was quantified using a secondary antibody labelled with horseradish peroxidase (HRP) (anti-IgG-HRP) catalyzed by 3,3′,5,5′-tetramethylbenzidine (TMB) mediator by chronoamperometry. A linear response was obtained in the range of 1:1000-1:200 v/v in phosphate buffer solution (PBS) and the limit of detection calculated was of 1:4947 v/v. The chronoamperometric method showed electrical signals directly proportional to antibody concentrations due to Ag-Ab specific and stable binding reaction.

Keywords: Immunosensor; SARS-CoV-2; N-protein

1. Introduction

The SARS-CoV-2 is the third species of betacoronavirus to cause outbreaks in recent decades, and the first to cause a high number of infected and deaths resulting from the effects of disease around the world [1]. COVID-19 is a disease caused by SARS-CoV-2, which affects billions of people in the world [2].

Covid-19 is a disease caused by SARS-CoV-2, which affects billions of people worldwide. Infections can be asymptomatic with mild flu-like symptoms, cough, fever, as well as severe complications that can lead to death. So, its detection is urgently necessary to effectively control the fast propagation of the virus since asymptomatic individuals can transmit the disease and therefore it is very important to identify and isolate [3, 4].

SARS-CoV-2 has spike proteins (S), membrane proteins (M), envelope proteins (E) and nucleocapsid proteins (N) in its structure. Thus, it has greater stability and less mutations over time. Moreover, these proteins are highly immunogenic and are expressed abundantly during infection, and have high specificity [5].

 doi:10.20944/preprints202210.0162.v1

For the detection of SARS-CoV-2, there are the conventional methods that can be highlighted the Reverse Transcription Polymerase Chain Reaction (RT-PCR) which is considered the gold standard for SARS-CoV-2 detection , enzyme-linked immunosorbent assay (ELISA), chemiluminescent immunoassay (CLIA), or through quick tests [6]. These conventional tests have limitations, such as high cost, time-consuming, need for a laboratory structure for its realization and the demand for an immunological window [7].

So, electrochemical biosensors appear as a promisor alternative to traditional methods, due to its exceptional analytical performance, small size and portability [8]. In addition, it can be used as diagnostic tool in a point of care, allowing a simple and quick detect the biomolecules in a complex sample matrix [9].

The electrochemical biosensors usually have been developed in screen-printed carbon electrodes (SPCE) to provide disposable devices. These SPCE are also easy to modify their surface with nanomaterials, contributing to their physical, chemical, and magnetic properties [8]. Among those used in biosensors, graphene can be highlighted, since it is usually constituted by functionalized groups, such as hydroxyls, epoxies, carbonyls, and carboxylic groups. The presence of these chemical compounds in their structure facilitates the immobilization of the bioreceptor, presenting an advantages in comparison with other namomaterials [10–12].

Thus, in this work, we propose an immunosensor based on SPCE modified with CG and N-protein for determination of IgG-SARS-CoV-2. Under optimized conditions, the immunosensor with electrochemical transducer achieved 0.02021% of detection limit

2. Materials and Methods

2.1. Reagents and Samples

Graphene nanoplatelets (XG sciences, USA), Sulfuric acid (H_2SO_4), nitric acid (H_2NO_3), disodium hydrogen phosphate (Na_2HPO_4), monosodium dihydrogen phosphate (NaH_2PO_4), 1-ethyl-3-[3-(dimethylamino)propyl]-carbodiimide (EDC), N-hydroxysuccinimide ester (NHS), bovine serum albumin (BSA) was purchased from Sigma-Aldrich and Merck Co. LLC (USA) and used without further purification. N-protein was synthetized and purified in Federal University of Amazonas [14]. 1-Step™ Ultra TMB-ELISA substrate was acquired from Thermo Fisher™ Scientific (USA). 0.1 mol L^{-1} PBS of pH 7 was prepared using Na_2HPO_4, NaH_2PO_4 and Milli-Q water. Besides, a solution containing 5 mmol L^{-1} $K_3Fe(CN)_6/K_4Fe(CN)_6$ with a ratio of 1:1 prepared in 0.1 mol L^{-1} KCl was used as redox probe in the electrochemical measurements. All the electrochemical experiments were performed at room temperature (22 ± 0.5 °C) and without stirring.

Due to the use of the N-protein as an IgG-specific antigen, the proposed method allows us to detect IgG in biological fluids without interfering with other biomolecules present in real samples. The human blood serum samples were provided from Federal University of Amazonas and this study was approved by The Research Ethics Committee of Federal University of Amazonas (CAAE:34906920.4.0000.5020) in accordance with Brazilian law, and the Declaration of Helsinki.

2.2. Apparatus and Procedures

The electrochemical measurements are obtained by Cyclic voltammetry (CV), electrochemical impedance spectroscopy (EIS) and chronoamperometry (CA) using an Autolab PGSTAT204 potentiostat/galvanostat equipped with FRA32M EIS module and NOVA software, 2.1.4 version (Metrohm Autolab, Netherlands). The commercial disposable SPCE from Metrohm Dropsens (Netherlands) was used as conductive support. They are composed of three electrodes, working electrode and counter electrode of carbon and reference pseudo-electrode of Ag/AgCl. CV was performed in a potential range between − 0.6 and 0.6 V, at scan rate of 50 mV s^{-1}. The EIS measurements were executed in frequency range of 10 kHz to 0.1 Hz at potential of 0.15 V and amplitude of 5 mV.

Preprints (www.preprints.org) | NOT PEER-REVIEWED | Posted: 12 October 2022 doi:10.20944/preprints202210.0162.v1

2.3. Assembly of the Biosensor

The biosensor fabrication steps, and its subsequent detection of IgG-SARS-CoV-2 antibodies are showed in Scheme 1. Prior to modification, the carbon surface was electrochemically activated with 0.5 mol L^{-1} H_2SO_4 by cyclic voltammetry technique, applying several potential between +1 and −1.5 V at scan rate of 100 mV s^{-1}[15–17]. For the preparation of the CG/SPCE, firstly, we prepared the CG through a carboxylation method in acid medium. For that, 7 mg of graphene was added to 30 mL of $H_2SO_{4(conc)}$, and 3 mg was added to 10 mL of $HNO_{3(conc)}$. In the end, both solutions were mixed and sonicated for 1 h. Afterwards, it was made a centrifugation for 1 h at 22 000 rpm, in order to wash five times the modified graphene with Milli-Q water. The main goal of this process was to neutralize the resulting graphene, until to achieved the pH 7 [18, 19]. The CG synthesized was then dried, using a rotary evaporation system.

The working electrode (WE) surface of the SPCE was modified with three layers of CG, being deposited 2 mg.mL^{-1} of CG solution by drop-casting, and dry at 60 °C. After that, the -COOH groups of the CG were activated through a carbodiimide reaction with 200 mM EDC and 100 mM NHS for 1 h at room temperature [20, 21]. After washing with PBS buffer, 3.82 µg.mL^{-1} of N-protein was immobilized on the WE surface for at least 180 min at 4 °C. The assembly of the biosensor was finalized with the blocking step, adding 1% BSA to the WE surface for 60 min at room temperature.

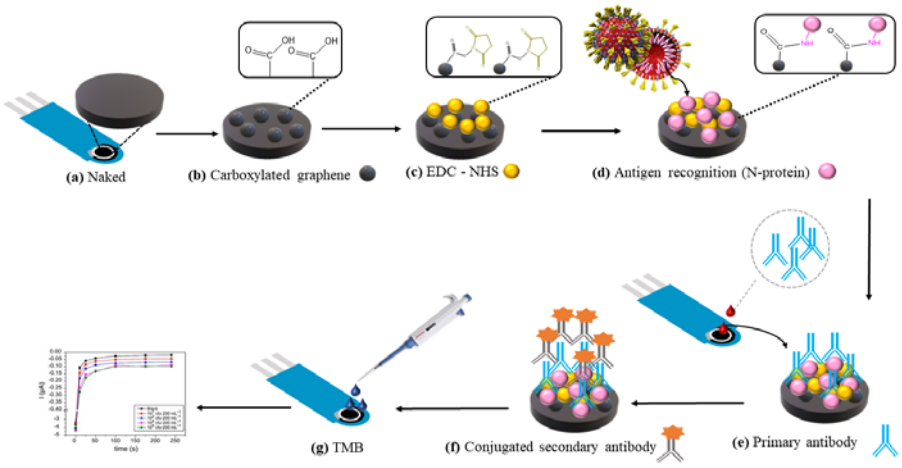

Scheme 1. Representation of the immunosensor assembly process and mechanism of indirect detection of analyte target.

2.2. Electrochemical Detection

The detection of antibodies was carried out by enzymatic reaction using TMB as substrate for 1 min in the dark. Firstly, the human serum sample (1:200 v/v prepared in PBS solution) was incubated for 30 min on the WE, followed by the addition of horseradish peroxidase-labeled anti-human IgG (anti-IgG-HRP) (1:1000 v/v prepared in PBS solution) for another 30 min at room temperature [22–24]. The enzymatic reaction occurs when TMB is added after the previous step. Chronoamperometric technique was used to follow the current associated to the oxidized TMB reduction process [25, 26] Thus, it is was applied a constant potential of −0.19 V during 50 s. The analytical signal was based on the absolute value of the current and was recorded at the end of the 20s. For IgG- SARS-CoV-2 detection using the immunosensor, the human serum samples were diluted in PBS, from

Preprints (www.preprints.org) | NOT PEER-REVIEWED | Posted: 12 October 2022 doi:10.20944/preprints202210.0162.v1

1:1000 to 1:200 and the response registered by CA. All measurements were made in triplicate. A new electrode/immunosensor was used for each measurement, which prevents fouling, non-specific adsorption, and reagent leaching. The samples were also analyzed in parallel through indirect ELISA method, which is used to measure anti-SARS-CoV-2 nucleocapsid immunoglobulin G (IgG) antibody as a reference method according LALWANI et al., 2021.

3. Results and Discussion

3.1

All steps of each modification on SPCEs surface were evaluated, since bare SPCE, CG/SPCE, EDC-NHS/CG/SPCE, N-protein/EDC-NHS/CG/SPCE to BSA/N-protein/EDC-NHS/CG/SPCE. The electrochemical response was followed by CV and EIS, using $[Fe(CN)_6]^{3-/4-}$ as a redox probe (Figure 1) to characterize the electrode surface after each modification step. As can be seen from the cyclic voltammograms (Figure 1 A), the anodic and cathodic peaks were registered in all electrode's modification steps.

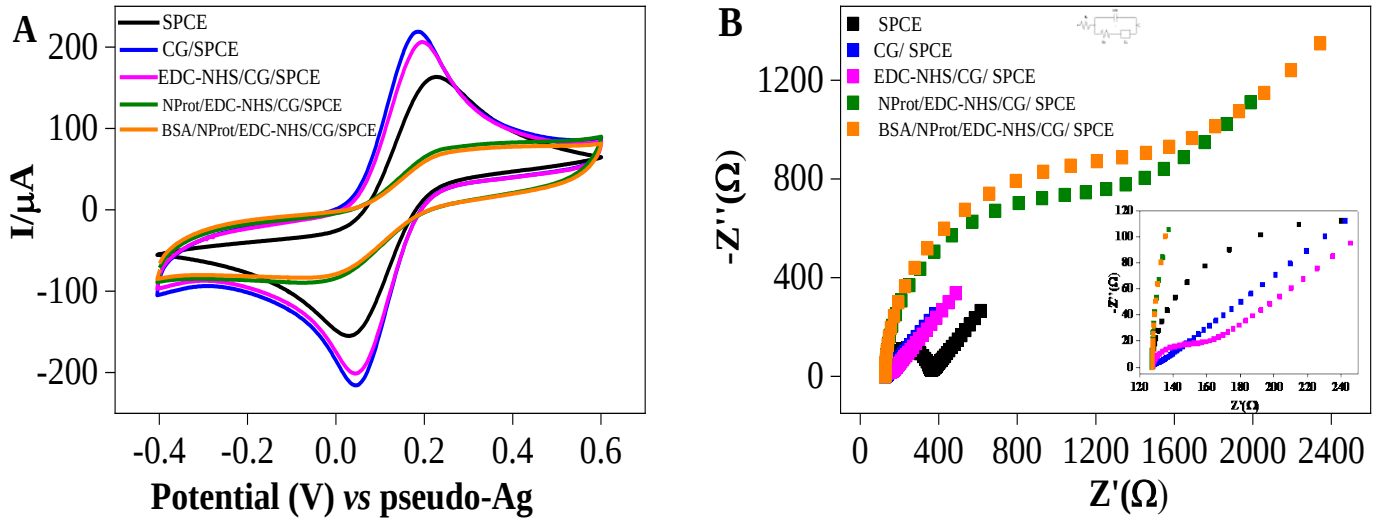

Figure 1. (A) Cyclic voltammograms and (B) EIS measurements of bare SPCE (black) CG/SPCE (blue), EDC-NHS/CG/SPCE (magenta), N-protein/EDC-NHS/CG/SPCE (green) and BSA/N-protein/EDC-NHS/CG/SPCE (orange) in 5 mmol L^{-1} $[Fe(CN)_6]^{3-/4-}$+ 0.1 mol L^{-1} KCl.

In the case of bare SPCE, the redox peaks exhibited a separation of ~0.2 V. After modification with CG, the current peaks from CG/SPCE increased approximately 30%. Moreover, the potential of anodic and cathodic peaks got closer to each other, showing a decrease in ΔEp about 0.14 V, which suggests an increment of electron transfer between electrochemical probe and modified surface of electrode. Consequently, the electrochemical performance of SPCE was improved. The activation of the carboxyl group on the SPCE surface with EDC-NHS (EDC-NHS/CG/SPCE), promoted a decrease in peak current. A possible explanation is the insulating feature of these molecules hinders the electron transfer from the substrate to the redox couple in the electrolyte interface [27, 28]. After the immobilization of antigen (N-protein) onto the electrode surface, the anodic peak current also decreased significatively to 71 µA. Maybe the reason is that the immobilized structures acted as electron transfer blocking layer, and it hindered the diffusion of $[Fe(CN)_6]^{3-/4-}$ redox probe toward the electrode surface. This result proved the success immobilizing of the antigen onto the electrode surface. In the blocking step with BSA (1%), there was a small decrease in current peaks in comparison to the previous step. It could be explained by the presence of more biological species on the electrode surface, which can prevent the

Preprints (www.preprints.org) | NOT PEER-REVIEWED | Posted: 12 October 2022 doi:10.20944/preprints202210.0162.v1

transfer of electrons. This result is expected since the purpose of BSA is to block free -COOH groups and avoid unspecific binding of antibodies in the detection step.

The EIS analysis (Figure 1 B) showed changes in resistance charge transfer represented in the Nyquist plot. The semicircle portion from high to intermediate frequencies refers to the kinetic charge transfer process whereas the straight line at low frequencies arises from the diffusional barrier regarding the redox couple mass-transfer [29]. The Rct value for the bare SPCE was 157 Ω, while N-protein/EDC-NHS/CG/SPCE and BSA/N-protein/EDC-NHS/CG/SPCE obtained 836 Ω and 1250 Ω, respectively. These changes indicate that each chemical modification on the electrode surface was successfully obtained. The increment in the diameter of the semicircle in the Nyquist plot can be attributed to the steric and resistive behavior of the molecules adhered to the electrode surface, corroborating the performance previously observed in cyclic voltammogram.

3.1. Optimization of Antigen Immobilization

For immobilization of N-protein step different incubation times (10, 20, 30, 60, 120, 180, 360, 720 e 1440 min) were tested. The electrochemical response was followed by CV and it is illustrated in Figure 2 A. The CV peak currents almost stabilized when the incubation time was higher than 180 min. Thus 180 min was chosen as the optimum immobilization time for the biosensor fabrication Figure 2 B.

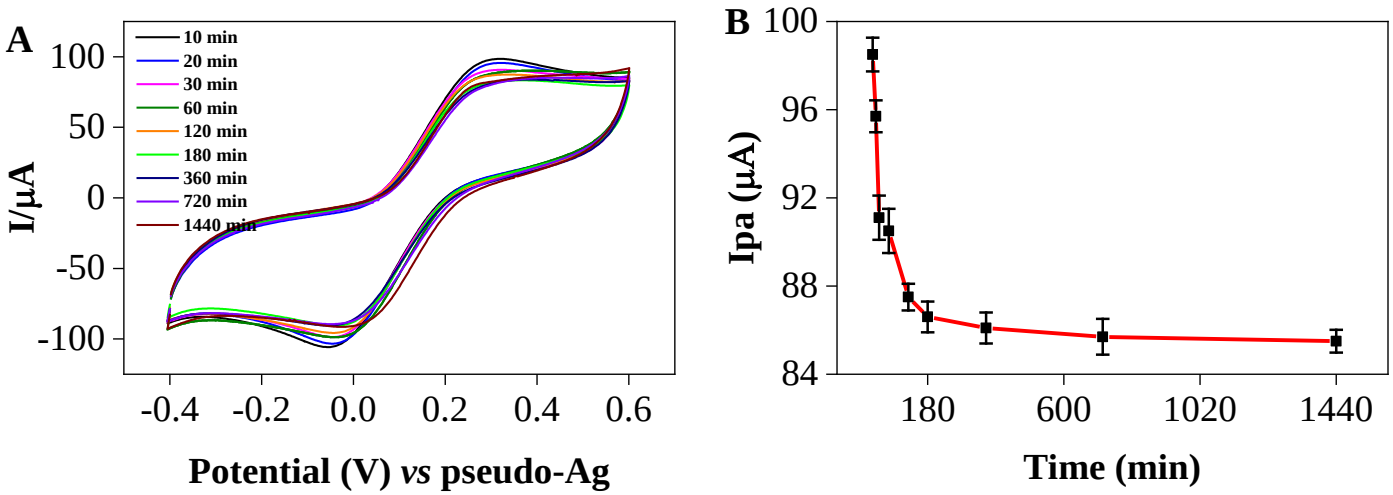

Figure 2. Optimization of N-protein immobilization time. (A) Cyclic voltammograms in 5 mmol L^{-1} $[Fe(CN)_6]^{3-/4-}$ + 0.1 mol L^{-1} KCl and (B) Plots of Ipa (µA) versus tempo (min).

3.2. Cyclic Voltammetric and Chronoamperometric Studies of TMB at SPCEs

CV was used to investigate the oxidation and reduction process of the TMB on a SPCE, by scanning the potential between −400 and 600 mV at scan rate of 50 mV s^{-1}. Figure 3 shows the cyclic voltammograms obtained for bare SPCE and CG/SPCE.

Preprints (www.preprints.org) | NOT PEER-REVIEWED | Posted: 12 October 2022 doi:10.20944/preprints202210.0162.v1

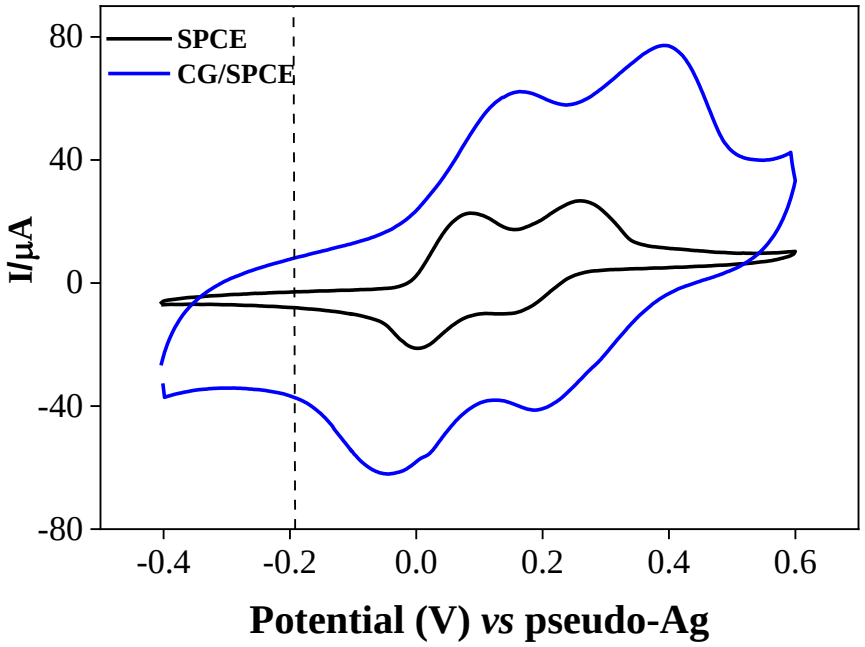

Figure 3. Cyclic voltammograms for SPCE (black) and CG/SPCE (blue) in TMB solution.

The results evidenced an increase in peak current in CG/SPCE (Ipa_I = 62.2 µA, Ipa_{II} = 76.8 µA, Ipc_I = −62.3 µA, Ipc_{II} = −41.4 µA) in comparison with bare SPCE (Ipa_I = 22.4 µA, Ipa_{II} = 26.2 µA, Ipc_I = −21.5 µA, Ipc_{II} = −9.4 µA) due to the high conductivity of CG composites that contribute to a faster electron transfer on the modified electrode. In the immunosensor format, the detection of HRP-labeled secondary antibody was based on the electrochemical reduction of TMB oxidized by enzymatic reaction. As previously described in the literature [23, 24, 29–40], TMB undergoes a two-electron oxidation-reduction process, which is characterized in our modified system (CG/SPCE) by two reduction peaks at 186 and -50 mV. Only the signal from oxidized TMB formed by HRP oxidation was required and this should be readily achieved by stepping the potential from open circuit to a suitable negative potential. This is not feasible using CV because any reduced TMB would be electrochemically oxidized at the initial potential, which would give an erroneous measurement for the resulting reduction peak [24]. Based on these observations, an applied potential of -0.19 V was chosen for subsequent chronoamperometric experiments, with the aim of efficiently reducing the oxidized TMB formed on the electrode surface. Such a detection mode was previously described in the literature [13, 24, 32, 37, 41, 42] for the development of immunosensors and genosensors.

3.3. Immunosensor Calibration

The most suitable electrochemical method to monitor oxidized TMB species was chronoamperometry. The analytical performance of Immunosensor was evaluated in human serum samples diluted in PBS. Under ideal conditions, each sample was incubated separately on the surface of the biodevice. Furthermore, its repeatability was investigated, which each sample was tested three times. The chronoamperograms discriminated qualitatively the presence of IgG-SARS-CoV-2 in negative reference serum and positive reference serum to test the viability of the immunosensor. PBS was used as a blank control (Figure 4).

Preprints (www.preprints.org) | NOT PEER-REVIEWED | Posted: 12 October 2022 doi:10.20944/preprints202210.0162.v1

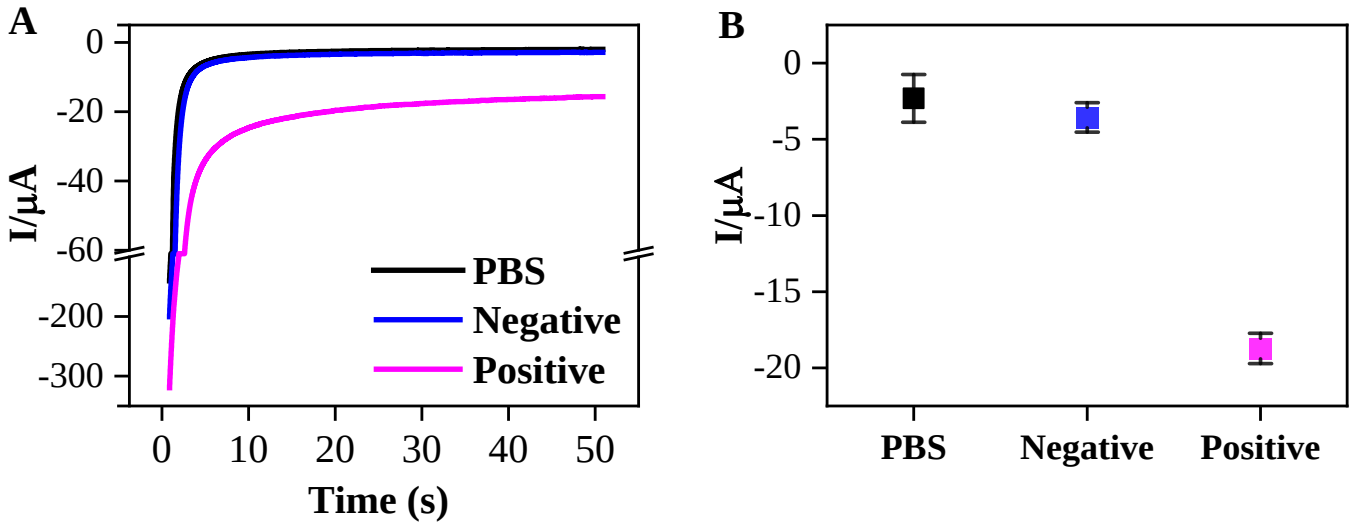

Figure 4. Chronoamperograms recorded with PBS, negative and positive controls. Applied potential of -0.19 V vs. pseudo-Ag.

As can be seen, the I-T curve showed that the steady-state signal was reached after 10 s. The steady-state current in the presence of IgG-SARS-CoV-2 was -18.72 µA, whereas for negative reference serum and PBS it was only -3.56 µA and -2.31 µA, respectively µA (Figure 4 A). The P/N ratio (~5.5) between positive reference serum and negative reference serum demonstrates the immunosensor's ability to distinguish IgG-SARS-CoV-2 patient serum from normal human serum. To test the system's ability to detect IgG-SARS-CoV-2 in human serum, various concentrations (1:200; 1:400; 1:600; 1:800 and 1:1000) were tested on the immunosensor. Once immunoassay and incubation with TMB substrate were performed, chronoamperometric measurements were performed at a reduction potential of -0.19 V vs. pseudo-Ag for a total of 50 s.

Figure 5 A exhibited a rapid decrease in current during the first 10 s resulting from electrode polarization, the reaction at the electrode stabilized and began to reach a plateau state. Furthermore, it was observed that the differences in the current values obtained by the different concentrations of serum human with IgG-SARS-CoV-2 were smaller, mainly at higher dilutions. This is clearly seen in Figure 5 B, where the current values were plotted against the concentration of serum human with IgG-SARS-CoV-2 at different reaction times. The results show a linear relationship between the concentration of serum human with IgG-SARS-CoV-2 and the current obtained in short measurement periods between 10 and 20 s. However, after 30 s of reaction, linearity was lost in the highest dilutions of serum human with IgG-SARS-CoV-2, probably because of electrode passivation related to TMB precipitation. When HRP oxidizes TMB, the resulting blue product is deposited on the surface of the electrode, blocking it, and reducing the current obtained. At high concentrations of labeled antibodies, TMB is oxidized more quickly and, therefore, the passivation effect is observed earlier. In addition to the loss of linearity, this may also explain the large standard deviations found at high concentrations of serum human with IgG-SARS-CoV-2 [24, 43, 44].

Preprints (www.preprints.org) | NOT PEER-REVIEWED | Posted: 12 October 2022 doi:10.20944/preprints202210.0162.v1

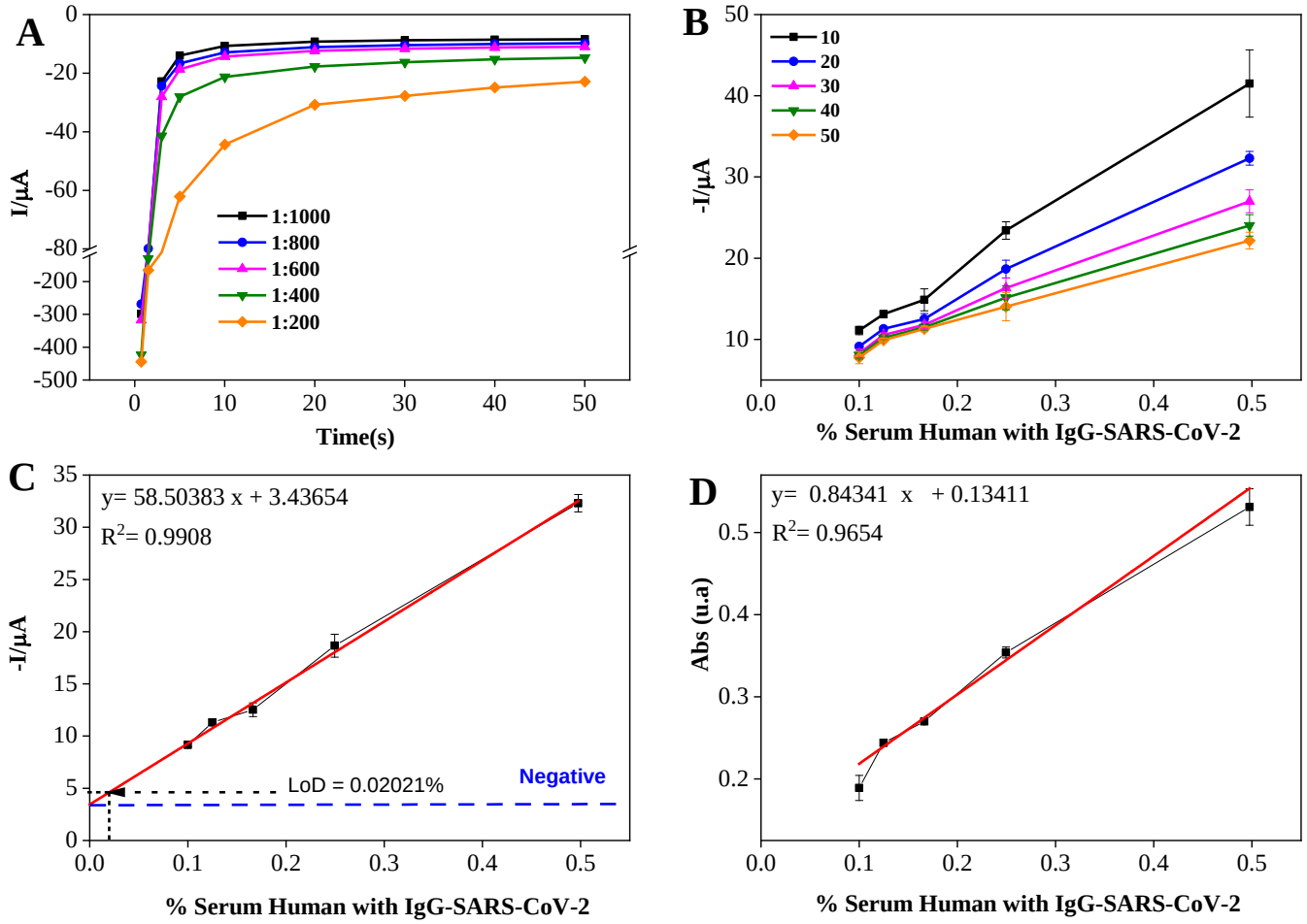

Figure 5. (A) Chronoamperometric response measured for different concentrations of human serum with IgG-SARS-CoV-2. (B) Current values registered from 10 to 50 s for different concentrations of serum human with IgG-SARS-CoV-2. Calibration curve for IgG-SARS-CoV-2 determination through (C) CA technique and (D) ELISA technique. Standard error bars correspond to correspond to measurements made on three replicates of each concentration (n = 3).

The indirect electrochemical assay was used to estimate the antibodies levels in serum sample. In Figure 5 C, the calibrations curves were plotted using absolute values of stable current recorded at time 20 s against the concentration of IgG-SARS-CoV-2 present in the samples. The Immunosensor performance was evaluated using serum human positive for SARS-CoV-2 concentrations from 1:1000; 1:800; 1:600; 1:400; 1:200. It is observed that the current values are proportionally to increase the concentration of IgG-SARS-CoV-2. The resulting average current values (n = 3) was established with regression equation: $y = 58.5038\,x + 3.43654$ According to the Miller and Miller method [26], the detection limit of our system was determined taking into account the variability of the chronoamperometric current that was obtained in positive samples (samples without IgG-SARS-CoV-2). This limit was established as a current value of 4.59 µA corresponding to a % concentration of IgG-SARS-CoV-2 of 0,02018% of IgG-SARS-CoV-2, which is equivalent to a dilution factor of 1:4954. A linear graph is obtained with R^2 of 0.9908, indicating that the time at 20 s is suitable for this study. The resolution of the curve fitting indicated a sensitivity (expressed as the slope of the I vs. % Serum Human with IgG-SARS-CoV-2) of 3.43654 /% Serum Human with IgG-SARS-CoV-2 in the range of 1:1000 to 1:200 v/v. As shown, the fabricated biodevice can be correctly used in the serum human sample.

 doi:10.20944/preprints202210.0162.v1

To confirm the results obtained by CA to detect IgG-SARS-CoV-2, experiments through ELISA technique were performed. The calibration curve (Figure 5 D) was obtained by plotting of Absorbance versus % Serum human with IgG-SARS-CoV-2. The results showed a linear relationship in the concentration range from 1:1000 to 1:200, with a LOD calculated of 1:2023 (0.04940%). The curve equation was defined as $y = 0.84341\ x + 0.13411$, com $R^2 = 0.9654$.

For the feasibility of biodevice in the detection of IgG-SARS-CoV-2 in biological samples, 10 clinical samples were also tested to verify the biodevice's viability in detecting IgG-SARS-CoV-2 antibody in biological samples and the results obtained are summarized in Table 1 and compared with the ELISA test. The results showed possible application of the biodevice to detect IgG-SARS-CoV-2 in blood serum samples.

Table 1. Detection of IgG-SARS-CoV-2 in blood serum samples using the proposed immunosensor and the ELISA test.

Patients	*Immunosensor*	*ELISA*
1	+	+
2	+	+
3	+	+
4	+	+
5	+	+
6	-	-
7	-	-
8	-	-
9	-	-
10	-	-

4. Conclusions

Effective monitoring and surveillance of Covid-19 in Primary Health Care is essential to prevent the emergence of outbreaks. In this work, a highly sensitive electrochemical immunosensor for IgG-SARS-CoV-2 nucleocapsid protein detection was successfully developed. Modification of SPCE with CG as sensor platform and implementation of indirect immunoassay format was successfully used for detection of IgG-SARS-CoV-2 nucleocapsid protein. The electrochemical study revealed the immobilization of Ag in SPCE/GC, the CG aimed to improve the electrochemical signal and the selectivity in the immobilization of the N-protein, indicating the suitability of this sensor platform to be developed as a biosensor. The low LOD (0.02021%) allows detecting smaller amounts of IgG-SARS-CoV-2 in real samples. In addition, concentration and immunodetection steps can be integrated into a single support soon, allowing for a more direct and faster system that provides results within 20 s. Thus, the detection system developed can overcome one of the most significant disadvantages of the ELISA method, the detection time. As a result, we achieved our goal of a fast, cost-effective, and easy-to-use system to detect IgG-SARS-CoV-2.

.

Author Contributions: L.F., C.R. and A.M.D.G.: Conceptualization, methodology, and data collecting/analysis, writing – original draft; Y.R-B., A.T., and B.S.: Methodology, Investigation, L.F..; Formal analysis, Methodology, Resources, M.G.S., J.L.; S.A-F., P.L. and W.B.; Writing — Original draft preparation, L.F., C.R. and A.M.D.G.; writing — review and editing, M.S..; S.A-F., P.L. and W.B.; visualization, Formal analysis, Investigation, supervision, M.G.S., J.L.; S.A-F., P.L. and W.B; funding

acquisition, W.B: Conceptualization, Formal analysis, Investigation, Methodology, Project administration, Resources, Supervision, Visualization, Writing – original draft, Writing – review & editing. All authors have read and agreed to the published version of the manuscript.

Funding: The authors would like to thank for the financial support to Universidade Federal do Amazonas (UFAM), Fundação de Amparo à Pesquisa do Estado do Amazonas (FAPEAM) and Instituto Leônidas e Maria Deane (ILMD/Fiocruz Amazônia). L.F. acknowledges financial support from theCoordenação de Aperfeiçoamento de Pessoal de Nível Superior (CAPES) [8888.452396/20019-01].

Institutional Review Board Statement: The study was conducted in accordance with the Declaration of Helsinki and approved by the Research Ethics Committee of Federal University of Amazonas (CAAE:34906920.4.0000.5020 - 15/10/2020).” for studies involving humans.

Informed Consent Statement: Informed consent was obtained from all subjects involved in the study. Written informed consent has been obtained from the patient(s) to publish this paper.

Data Availability Statement: The data presented in this study are available in DOI: 10.1016/j.ijid.2021.07.017

Acknowledgments: The authors thank the Laboratory of Bioelectronics and Electroanalytics (LABEL/UFAM) and Laboratory of Immunology and Infectious Diseases (UFAM/FioCruz).

Conflicts of Interest: There are no conflicts to declare.

References

1. Dhama, Ck.; Khan, S.; Tiwari, R.; Sircar, S.; Bhat, S.; Malik, Y.S.; Singh, K.P.; Chaicumpa, W.; Bonilla-Aldana, D.K.; Rodriguez-Morales, A.J. Coronavirus Disease 2019-COVID-19, *Clin. Microbiol. Rev.*, **2020**, *33*, 1–48, DOI: 10.1128/CMR.00028-20.
2. OMS.*Archived: WHO Timeline - COVID-19*. https://www.who.int/news/item/27-04-2020-who-timeline---covid-19 (accessed on 11/04/2021).
3. Hoehl, S.; Rabenau, H.; Berger, A.; Kortenbusch, M.; Cinatl, J.; Bojkova, D.; Behrens, P.; Böddinghaus, B.; Götsch, U.; Naujoks, F.; Neumann, P.; Schork, J.; Tiarks-Jungk, P.; Walczok, A.; Eickmann, M.; Vehreschild, M.J.G.T.; Kann, G.; Wolf, T.; Gottschalk, R.; Ciesek, S. Evidence of SARS-CoV-2 Infection in Returning Travelers from Wuhan, China, *N. Engl. J. Med.*, **2020**, *382*, 1278–1280, DOI: 10.1056/nejmc2001899.
4. Yu, P.; Zhu, J.; Zhang, Z.; Han, Y. A familial cluster of infection associated with the 2019 novel coronavirus indicating possible person-to-person transmission during the incubation period, *J. Infect. Dis.*, **2020**, *221*, 1757–1761, DOI: 10.1093/infdis/jiaa077.
5. Dutta, N.K.; Mazumdar, K.; Gordy, J.T. The Nucleocapsid Protein of SARS–CoV-2: a Target for Vaccine Development, *J. Virol.*, **2020**, *94*, DOI: 10.1128/jvi.00647-20.
6. Döhla, M.; Boesecke, C.; Schulte, B.; Diegmann, C.; Sib, E.; Richter, E.; Eschbach-Bludau, M.; Aldabbagh, S.; Marx, B.; Eis-Hübinger, A.M.; Schmithausen, R.M.; Streeck, H. Rapid point-of-care testing for SARS-CoV-2 in a community screening setting shows low sensitivity, *Public Health*, **2020**, *182*, 170–172, DOI: 10.1016/j.puhe.2020.04.009.
7. *Testes para a Covid-19: como são e quando devem ser feitos*. https://portal.fiocruz.br/noticia/testes-para-covid-19-como-sao-e-quando-devem-ser-feitos (accessed on 09/09/2022).
8. Mehrotra, P. Biosensors and their applications - A review, *J. Oral Biol. Craniofacial Res.*, **2016**, *6*, 153–159, DOI: 10.1016/j.jobcr.2015.12.002.
9. Rahmati, Z.; Roushani, M.; Hosseini, H.; Choobin, H. An electrochemical immunosensor using SARS-CoV-2 spike protein-nickel hydroxide nanoparticles bio-conjugate modified SPCE for ultrasensitive detection of SARS-CoV-2 antibodies, *Microchem. J.*, **2021**, *170*, 106718, DOI: 10.1016/j.microc.2021.106718.
10. Mincu, N.B.; Lazar, V.; Stan, D.; Mihailescu, C.M.; Iosub, R.; Mateescu, A.L. Screen-Printed Electrodes (SPE) for in vitro diagnostic purpose, *Diagnostics*, **2020**, *10*, 1–21, DOI: 10.3390/diagnostics10080517.
11. Rabchinskii, M.K.; Shnitov, V. V.; Stolyarova, D.Y.; Ryzhkov, S.A.; Baidakova, M. V.; Lobanova, E.Y.; Shvidchenko, A. V.;

Besedina, N.A.; Smirnov, D.A. Graphene oxide conversion into controllably carboxylated graphene layers via photoreduction process in the inert atmosphere, *Fullerenes Nanotub. Carbon Nanostructures*, **2020**, *28*, 221–225, DOI: 10.1080/1536383X.2019.1686625.

12. Kuila, T.; Bose, S.; Mishra, A.K.; Khanra, P.; Kim, N.H.; Lee, J.H. Chemical functionalization of graphene and its applications, *Prog. Mater. Sci.*, **2012**, *57*, 1061–1105, DOI: 10.1016/j.pmatsci.2012.03.002.
13. Lee, G.Y.; Park, J.H.; Chang, Y.W.; Cho, S.; Kang, M.J.; Pyun, J.C. Chronoamperometry-Based Redox Cycling for Application to Immunoassays, *ACS Sensors*, **2018**, *3*, 106–112, DOI: 10.1021/acssensors.7b00681.
14. Lalwani, P.; Salgado, B.B.; Filho, I.V.P.; da Silva, D.S.S.; de Morais, T.B. do N.; Jordão, M.F.; Barbosa, A.R.C.; Cordeiro, I.B.; Neto, J.N. de S.; de Assunção, E.N.; dos Santos, R.O.; Carvalho, N.O.; Sobrinho, W.B.S.; da Costa, C.F.; de Souza, P.E.; de Albuquerque, B.C.; Ganoza, C.A.; Araujo-Castillo, R. V.; Filho, S.A.; Lalwani, J.D.B. SARS-CoV-2 seroprevalence and associated factors in Manaus, Brazil: baseline results from the DETECTCoV-19 cohort study, *Int. J. Infect. Dis.*, **2021**, *110*, 141–150, DOI: 10.1016/j.ijid.2021.07.017.
15. Hayat, A.; Barthelmebs, L.; Sassolas, A.; Marty, J.L. An electrochemical immunosensor based on covalent immobilization of okadaic acid onto screen printed carbon electrode via diazotization-coupling reaction, *Talanta*, **2011**, *85*, 513–518, DOI: 10.1016/j.talanta.2011.04.034.
16. Stanković, V.; Đurđić, S.; Ognjanović, M.; Antić, B.; Kalcher, K.; Mutić, J.; Stanković, D.M. Anti-human albumin monoclonal antibody immobilized on EDC-NHS functionalized carboxylic graphene/AuNPs composite as promising electrochemical HSA immunosensor, *J. Electroanal. Chem.*, **2020**, *860*, 1–7, DOI: 10.1016/j.jelechem.2020.113928.
17. Cui, G.; Jae Hyun Yoo; Joung Su Lee; Yoo, J.; Jung Hee Uhm; Geun Sig Cha; Nam, H. Effect of pre-treatment on the surface and electrochemical properties of screen-printed carbon paste electrodes, *Analyst*, **2001**, *126*, 1399–1403, DOI: 10.1039/b102934g.
18. Verdoodt, N.; Basso, C.R.; Rossi, B.F.; Pedrosa, V.A. Development of a rapid and sensitive immunosensor for the detection of bacteria, *Food Chem.*, **2017**, *221*, 1792–1796, DOI: 10.1016/j.foodchem.2016.10.102.
19. Jaiswal, N.; Pandey, C.M.; Soni, A.; Tiwari, I.; Rosillo-Lopez, M.; Salzmann, C.G.; Malhotra, B.D.; Sumana, G. Electrochemical genosensor based on carboxylated graphene for detection of water-borne pathogen, *Sensors Actuators, B Chem.*, **2018**, *275*, 312–321, DOI: 10.1016/j.snb.2018.07.055.
20. Ngunjiri, J.N.; Stark, D.J.; Tian, T.; Briggman, K.A.; Garno, J.C. Immobilization of proteins on carboxylic acid functionalized nanopatterns, *Anal. Bioanal. Chem.*, **2013**, *405*, 1985–1993, DOI: 10.1007/s00216-012-6621-3.
21. Nakajima, N.; Ikada, Y. Mechanism of Amide Formation by Carbodiimide for Bioconjugation in Aqueous Media, *Bioconjug. Chem.*, **1995**, *6*, 123–130, DOI: 10.1021/bc00031a015.
22. Mavrikou, S.; Moschopoulou, G.; Zafeirakis, A.; Kalogeropoulou, K.; Giannakos, G.; Skevis, A.; Kintzios, S. An ultra-rapid biosensory point-of-care (POC) assay for prostate-specific antigen (PSA) detection in human serum, *Sensors (Switzerland)*, **2018**, *18*, 1–14, DOI: 10.3390/s18113834.
23. Baldrich, E.; del Campo, F.J.; Muñoz, F.X. Biosensing at disk microelectrode arrays. Inter-electrode functionalisation allows formatting into miniaturised sensing platforms of enhanced sensitivity, *Biosens. Bioelectron.*, **2009**, *25*, 920–926, DOI: 10.1016/j.bios.2009.09.009.
24. Ezenarro, J.J.; Párraga-Niño, N.; Sabrià, M.; Del Campo, F.J.; Muñoz-Pascual, F.X.; Mas, J.; Uria, N. Rapid detection of legionella pneumophila in drinking water, based on filter immunoassay and chronoamperometric measurement, *Biosensors*, **2020**, *10*, DOI: 10.3390/bios10090102.
25. Biscay, J.; García, M.B.G.; García, A.C. Electrochemical biotin determination based on a screen printed carbon electrode array and magnetic beads, *Sensors Actuators, B Chem.*, **2014**, *205*, 426–432, DOI: 10.1016/j.snb.2014.08.042.
26. Pérez-Fernández, B.; Mercader, J. V.; Abad-Fuentes, A.; Checa-Orrego, B.I.; Costa-García, A.; Escosura-Muñiz, A. de la. Direct

competitive immunosensor for Imidacloprid pesticide detection on gold nanoparticle-modified electrodes, *Talanta*, **2020**, *209*, 120465, DOI: 10.1016/j.talanta.2019.120465.

27. Lamarca, R.S.; Faria, R.A.D. De; Zanoni, M.V.B.; Nalin, M.; Lima Gomes, P.C.F. De; Messaddeq, Y. Simple, fast and environmentally friendly method to determine ciprofloxacin in wastewater samples based on an impedimetric immunosensor, *RSC Adv.*, **2020**, *10*, 1838–1847, DOI: 10.1039/c9ra09083e.
28. Tsai, J.Z.; Chen, C.J.; Settu, K.; Lin, Y.F.; Chen, C.L.; Liu, J.T. Screen-printed carbon electrode-based electrochemical immunosensor for rapid detection of microalbuminuria, *Biosens. Bioelectron.*, **2016**, *77*, 1175–1182, DOI: 10.1016/j.bios.2015.11.002.
29. Ahammad, A.J.S. Hydrogen Peroxide Biosensors Based on Horseradish Peroxidase and Hemoglobin, *J. Biosens. Bioelectron.*, **2012**, *s9*, 1–11, DOI: 10.4172/2155-6210.S9-001.
30. Urban, P.L.; Goodall, D.M.; Bruce, N.C. Enzymatic microreactors in chemical analysis and kinetic studies, *Biotechnol. Adv.*, **2006**, *24*, 42–57, DOI: 10.1016/j.biotechadv.2005.06.001.
31. Cawthraw, S.A.; Feldman, R.A.; Sayers, A.R.; Newell, D.G. Long-term antibody responses following human infection with Campylobacter jejuni, *Clin. Exp. Immunol.*, **2002**, *130*, 101–106, DOI: 10.1046/j.1365-2249.2002.02043.x.
32. Fanjul-Bolado, P.; González-García, M.B.; Costa-García, A. Amperometric detection in TMB/HRP-based assays, *Anal. Bioanal. Chem.*, **2005**, *382*, 297–302, DOI: 10.1007/s00216-005-3084-9.
33. Volpe, G.; Compagnone, D.; Draisci, R.; Palleschi, G. 3,3′,5,5′-Tetramethylbenzidine as electrochemical substrate for horseradish peroxidase based enzyme immunoassays. A comparative study, *Analyst*, **1998**, *123*, 1303–1307, DOI: 10.1039/a800255j.
34. Li, J.; Lillehoj, P.B. Microfluidic Magneto Immunosensor for Rapid, High Sensitivity Measurements of SARS-CoV-2 Nucleocapsid Protein in Serum, *ACS Sensors*, **2021**, *6*, 1270–1278, DOI: 10.1021/acssensors.0c02561.
35. Marquez, L.A.; Dunford, H.B. Mechanism of the oxidation of 3,5,3′,5′-tetramethylbenzidine by myeloperoxidase determined by transient- and steady-state kinetics, *Biochemistry*, **1997**, *36*, 9349–9355, DOI: 10.1021/bi970595j.
36. Lin, Y.Y.; Liu, G.; Wai, C.M.; Lin, Y. Magnetic beads-based bioelectrochemical immunoassay of polycyclic aromatic hydrocarbons, *Electrochem. commun.*, **2007**, *9*, 1547–1552, DOI: 10.1016/j.elecom.2007.02.007.
37. Josephy, P.D.; Eling, T.; Mason, R.P. The horseradish peroxidase-catalyzed oxidation of 3,5,3′,5′-tetramethylbenzidine. Free radical and charge-transfer complex intermediates., *J. Biol. Chem.*, **1982**, *257*, 3669–3675, DOI: 10.1016/s0021-9258(18)34832-4.
38. Talib, N.A.A.; Salam, F.; Sulaiman, Y. Development of highly sensitive immunosensor for clenbuterol detection by using poly(3,4-ethylenedioxythiophene)/graphene oxide modified screen-printed carbon electrode, *Sensors (Switzerland)*, **2018**, *18*, DOI: 10.3390/s18124324.
39. Hu, T.; Zhang, L.; Wen, W.; Zhang, X.; Wang, S. Enzyme catalytic amplification of miRNA-155 detection with graphene quantum dot-based electrochemical biosensor, *Biosens. Bioelectron.*, **2016**, *77*, 451–456, DOI: 10.1016/j.bios.2015.09.068.
40. Guo, L.; Xu, S.; Ma, X.; Qiu, B.; Lin, Z.; Chen, G. Dual-color plasmonic enzyme-linked immunosorbent assay based on enzyme-mediated etching of Au nanoparticles, *Sci. Rep.*, **2016**, *6*, 1–7, DOI: 10.1038/srep32755.
41. Heurich, M.; Kadir, M.K.A.; Tothill, I.E. An electrochemical sensor based on carboxymethylated dextran modified gold surface for ochratoxin A analysis, *Sensors Actuators, B Chem.*, **2011**, *156*, 162–168, DOI: 10.1016/j.snb.2011.04.007.
42. Bettazzi, F.; Natale, A.R.; Torres, E.; Palchetti, I. Glyphosate determination by coupling an immuno-magnetic assay with electrochemical sensors, *Sensors (Switzerland)*, **2018**, *18*, 1–12, DOI: 10.3390/s18092965.
43. Kim, S.D.; Chung, J.W.; Kim, J.T.; Krause, H.; Pyun, J.C. Gold-film array-electrode for electrochemical ELISA, *Sensors Actuators, B Chem.*, **2005**, *111–112*, 463–469, DOI: 10.1016/j.snb.2005.03.057.
44. Liu, M.; Zhang, Y.; Chen, Y.; Xie, Q.; Yao, S. EQCM and in situ FTIR spectroelectrochemistry study on the electrochemical oxidation of TMB and the effect of large-sized anions, *J. Electroanal. Chem.*, **2008**, *622*, 184–192, DOI:

 doi:10.20944/preprints202210.0162.v1

10.1016/j.jelechem.2008.06.002.